Density functional versus spin-density functional and the choice of correlated subspace in multivariable effective action theories of electronic structure

Hyowon Park, Andrew J. Millis, and Chris A. Marianetti

Phys. Rev. B **92**, 035146 — Published 27 July 2015

DOI: 10.1103/PhysRevB.92.035146

Density functional versus spin-density functional and the choice of correlated subspace in multi-variable effective action theories of electronic structure

Hyowon Park,[1,2,*] Andrew J. Millis,[2] and Chris A. Marianetti[1]

[1] *Department of Applied Physics and Applied Mathematics, Columbia University, New York, NY 10027, USA*

[2] *Department of Physics, Columbia University, New York, NY 10027, USA*

(Dated: July 6, 2015)

Modern extensions of density functional theory such as the density functional theory plus U and the density functional theory plus dynamical mean-field theory require choices, including selection of variable (charge vs spin density) for the density functional and specification of the correlated subspace. This paper examines these issues in the context of the "plus U" extensions of density functional theory, in which additional correlations on specified correlated orbitals are treated using a Hartree-Fock approximation. Differences between using charge-only or spin-density-dependent exchange-correlation functionals and between Wannier and projector-based definitions of the correlated orbitals are considered on the formal level and in the context of the structural energetics of the rare earth nickelates. It is demonstrated that theories based on spin-dependent exchange-correlation functionals can lead to large and in some cases unphysical effective on-site exchange couplings. Wannier and projector-based definitions of the correlated orbitals lead to similar behavior near ambient pressure, but substantial differences are observed at large pressures. Implications for other beyond density functional methods such as the combination of density functional and dynamical mean field theory are discussed.

I. INTRODUCTION

Modern theories of electronic structure can be formally constructed in terms of functionals of observables of interest whose stationary points deliver the values of the observables[1]. Practical use of this formal construction requires a choice of variables and of approximations to the functional. Perhaps the most common choice is density functional theory[2,3] (DFT), which can be formulated as an effective action that is a functional only of the electron density[4] (ie. not spin resolved). While DFT is in principle exact, existing approximations have had difficulty capturing phenomena related to the formation of local magnetic moments. For example, neither the local density approximation[3] (LDA) nor the generalized gradient approximation (GGA)[5] provide correct accounts of the structural energetics of layered and spinel manganites that exhibit cooperative Jahn-Teller distortions associated with the high spin state of Mn^{3+},[6] because at ambient pressure both LDA and GGA incorrectly predict that the Mn ion is in a nominal $|t_{2g}^4 e_g^0\rangle$ low-spin configuration instead of the proper high-spin $|t_{2g}^3 e_g^1\rangle$ state. Indeed it seems intuitively clear that it would be prohibitively difficult to construct a functional based only on the density that could capture this sort of effect, while a functional of the spin-density might have a robust approximation which can capture this physics. Additionally, a functional of the spin-density will clearly allow predictions to be made about magnetism, and this avenue has been pursued since the inception of DFT[3,7].

Functionals of both the charge and spin density such as the the local spin-density approximation (LSDA)[7–9] and the spin-dependent generalized gradient approximation (SGGA)[10,11] have been constructed. Such theories are often refered to as density functional theories, but in this paper we strictly distinguish terms, using the term density functional theory (DFT) to refer to theories such as the LDA and GGA that are based on a functional of the density only, and referring to theories such as the local spin density approximation (LSDA) or the spin-dependent GGA (SGGA) as spin-density functional theories (SDFT).

SDFT theories perform far better than DFT theories in describing the energetics of magnetic insulators, resolving, for example, the problems with manganites noted above.[6] SDFT theories additionally make predictions about spin magnitudes and the nature of ordered states. However, the known implementations of SDFT fail to correctly describe many aspects of the physics and structure of strongly correlated electron systems, for example providing qualitatively incorrect structures for the rare-earth nickelates[12,13] (see, e.g. Ref. 1 for additional examples).

These difficulties motivated the construction of new effective action theories that depend not only on the density or the spin-density, but also on additional properties of a subspace of orbitals for which correlations are believed to be relevant[1,14]. Subspaces which have been treated in this way include the transition metal d orbitals in transition metal oxides and the lanthanide/actinide f levels in heavy fermion compounds. Various different variables can be defined from the subspace of correlated orbitals. In this paper we focus on the historically important and currently widely used choice of the site-local spin and orbitally resolved density matrix associated with the correlated subspace[15]; however, we expect that our findings are relevant to other variable choices; in particular to the case of dynamical mean field theory where the additional variables are the components of the local Green's function. A straightforward functional

to use with the local spin-resolved density matrix is the Hartree-Fock energy functional, defined using site-local matrix elements of the Coulomb interaction. The functional resulting from this combination of a local Hartree-Fock functional of a correlated subspace and a standard functional of the density or spin-density is commonly referred to as a "+U" extension of density functional theory.

The paper that introduced the "+U" approach[14] employed a functional of the electron density only, so is referred to here as a DFT+U approach. However, the vast majority of subsequent papers[15] employ SDFT functionals and are referred to here as SDFT+U approaches. Despite the many successes of the +U methodology, basic points including the rationale for choosing SDFT+U in preference to DFT+U and the factors influencing the construction of the correlated subspace have not been clearly discussed. While the general formalism may be applied with any choice of orbital, it is important in practice to choose orbitals that are optimal in the context of the other approximations used in constructing the theory. While there is no clear prescription for doing this, the local nature of the approximations which will ultimately be used suggests that it is sensible to choose the correlated subspace to consist of well localized 'atomic-like' orbitals. These orbitals may be constructed from by projecting onto a set of localized orbitals defined to lie within atomic spheres. This choice is natural, given that many basis sets for electronic structure already utilize projectors. Projectors are used in various beyond-DFT methods including (S)DFT+U[16] as well as DFT+DMFT[17–23]. Alternatively, Wannier functions may be used to construct the correlated orbital sets for beyond DFT calculations. Various forms of the Wannier function have been used for DFT+U[24] and DFT+DMFT[25–32] including the projected Wannier function, Nth-order muffin-tin orbitals[24], and the maximally localized Wannier function (MLWF)[33–35].

In this paper we describe the physical differences between DFT+U and SDFT+U and provide guidelines to enable researchers to choose between them. We further compare the effect of different correlated orbitals sets (Projector vs Wannier) on energy calculations within the (S)DFT+U method. We also present a comprehensive discussion of the issues arising when the +U methodologies are combined with the Projector Augmented Plane Wave (PAW) formalism widely used to perform efficient (S)DFT calculations. In addition to the formalism we provide a quantitative application in the context of the relation between crystal structure and energetics of the rare-earth nickelates. This family of materials provides a useful benchmark because its members exhibit a structural phase transition which is not correctly captured either by DFT or by SDFT calculations. We compare DFT+U and SDFT+U, using both projectors and Wannier functions to construct the correlated subspace. These results can also be directly compared to our recent DFT+DMFT total energy calculations for the same class of materials[13].

We note in passing that an additional important issue in DFT+U and SDFT+U theories is the so-called double counting correction, introduced to account for the fact that the local interactions denoted by U and J are to some degree present already in the (S)DFT. The double counting issue has been addressed in great detail in previous work[13] and is not critical to the issues examined here. Therefore in this paper we use the conventional definition of the "fully localized-limit" double-counting[36,37].

The rest of this paper is organized as follows. Section II presents the basic formalism. Section III provides a careful discussion of the issues involved in combining the +U formalism with the projector augmented plane wave method. Section IV presents expressions for forces, needed in optimizing structures. Section V compares the DFT+U and SDFT+U (with projector and Wannier definitions of the correlated subspace) predictions for the structural properties of the rare earth nickelates as a function of unit cell volume, while section VIII provides a comparison of predictions for the rare earth nickelate phase diagram and the equilibrium volume. Section IX contains a summary and conclusions. Relevant computational details are given in Appendix A.

II. FORMALISM

In this section we present explicit formulae for the energy functional, using a variant of presentation of the DFT+DMFT functional given in Ref. 13. We derive the total energy functional for SDFT+U, and then obtain the DFT+U functional as a special case.

The SDFT+U total energy functional is defined by

$$E[\rho^\sigma, n^{\tau\sigma}] = \mathbf{Tr}[\langle \hat{H}_U^\sigma \rangle] - \mathbf{Tr}[\hat{V}_{Hxc}^\sigma \cdot \rho^\sigma] - \mathbf{Tr}[\hat{V}_{int}^\sigma \cdot n^{\tau\sigma}] + E^{Hxc}[\rho^\sigma] + E^{int}[n^{\tau\sigma}] \quad (1)$$

where ρ^σ denotes the charge density of electrons with spin σ (we neglect spin-orbit coupling here for simplicity) and $n^{\tau\sigma}$ is a density matrix within the correlated subspace of an atom τ. Here the bracket $\langle\rangle$ means that the eigenstates of $\hat{H}_U^\sigma$ are summed over for the eigenvalues less than the Fermi energy.

The functional E^{Hxc} is the familiar Hartree and exchange-correlation energy functional of the DFT theory to be used and $\hat{V}_{Hxc}^\sigma = \delta E^{Hxc}/\delta\rho^\sigma$ is the corresponding Hartree-exchange-correlation potential.

E^{int} is the combination of a Hartree-Fock potential energy E^{pot} defined within the correlated subspace and a double counting correction E^{DC} introduced to remove from this potential the parts already included in the underlying DFT:

$$E^{int} = E^{pot} - E^{DC}. \quad (2)$$

In the applications presented here we follow the common practice in the literature by choosing the correlated

subspace to be particular orbitals m of spin σ on particular atoms τ in the solid; for example the $3d$ orbitals in a first row transition metal ion or the $4f$ orbitals in a lanthanide ion, so that

$$E^{pot} = \sum_{\substack{\tau, m_1 m_2 \\ m_3 m_4 \sigma_1 \sigma_2}} (U^{\sigma_1\sigma_2\sigma_1\sigma_2}_{m_1 m_3 m_2 m_4} - U^{\sigma_1\sigma_2\sigma_2\sigma_1}_{m_1 m_3 m_4 m_2} \cdot \delta_{\sigma_1\sigma_2}) n^{\tau\sigma_1}_{m_1 m_2} n^{\tau\sigma_2}_{m_3 m_4} \tag{3}$$

where the $U^{\sigma_1\sigma_2\sigma_1\sigma_2}_{m_1 m_3 m_2 m_4}$ are the site-local matrix elements of the Coulomb interaction within the correlated subspace, appropriately renormalized by the solid-state environment. This paper will present an application of the formalism to the case of transition metal d-orbitals where (if spin orbit coupling is neglected), the $U^{\sigma_1\sigma_2\sigma_1\sigma_2}_{m_1 m_3 m_2 m_4}$ may be parametrized by the Slater integrals F^0, F^2, and F^4. We typically further assume that the d-wave functions are sufficiently similar to their free-space forms that $F^4 = 0.625F^2$. It is then conventional to define on-site interaction U and the Hund's coupling J via $F^0 = U$, $F^2 = (14/1.625)J$.[36]

The double counting energy E^{DC} is the subject of continuing discussion in the literature but these subtleties are not relevant here. We adopt the 'fully localized limit' form given by

$$E^{DC}[N^\sigma_\tau] = \frac{U}{2} N_\tau (N_\tau - 1) - \frac{J}{2} \sum_\sigma N^\sigma_\tau (N^\sigma_\tau - 1), \tag{4}$$

where N^σ_τ is the total number of electrons of spin σ on site τ and $N_\tau = \sum_\sigma N^\sigma_\tau$ is the total on-site charge density in the correlated subspace. Note that use of SDFT (in other words the dependence of $E^{Hxc}[\rho^\sigma]$ on the spin density) means that that the double counting potential E^σ_{DC} in Eq. 4 also depends on spin indices.

The corresponding interaction potential $\hat{V}^\sigma_{int}$ is obtained as $V^\sigma_{int} = \partial E^{int}/\partial n^{\tau\sigma}$:

$$\hat{V}^\sigma_{int} = \sum_{m,m'} |\tau, m, \sigma\rangle (V^{\tau\sigma}_{pot,mm'} - V^{\tau\sigma}_{DC}) \langle \tau, m', \sigma|, \tag{5}$$

where

$$V^{\tau\sigma}_{pot,mm'} = \sum_{m_1 m_2 \sigma_1} (U_{m_1 m m_2 m'} - U_{m_1 m m' m_2} \cdot \delta_{\sigma_1\sigma}) n^{\tau\sigma_1}_{m_1 m_2} \tag{6}$$

and

$$V^{\tau\sigma}_{DC} = U(N_d - \frac{1}{2}) - J(N^\sigma_d - \frac{1}{2}). \tag{7}$$

Finally, the effective Hamiltonian $\hat{H}^\sigma_U$ is

$$\hat{H}^\sigma_U = \hat{H}^\sigma_{KS} + \hat{V}^\sigma_{int}, \tag{8}$$

where the Kohn-Sham Hamiltonian $\hat{H}^\sigma_{KS}$ is

$$\hat{H}^\sigma_{KS}[\rho^\sigma, \mathbf{R}] = -\frac{1}{2}\hat{\nabla}^2 + \hat{V}_{ext}[\mathbf{R}] + \hat{V}^\sigma_{Hxc}[\rho^\sigma]. \tag{9}$$

$\hat{H}^\sigma_U$ is the analogue of the Kohn-Sham Hamiltonian $\hat{H}^\sigma_{KS}$ of SDFT. $\hat{V}_{ext}$ is an external potential arising from atomic nuclei at the position $\mathbf{R}$ (the interaction between nuclei is not explicitly denoted but is included in the formalism).

The physical state of the system at zero temperature is obtained by extremizing Eq. 1 with respect to variations in ρ^σ and $n^{\tau\sigma}$. To perform the extremization, we solve the eigenvalue problem of $\hat{H}^\sigma_U$ and find the eigenstates $|\Psi^\sigma_{i\mathbf{k}}\rangle$ (i is a band index and k is a momentum in the first Brillouin zone). We then determine the local charge density $\rho^\sigma(\mathbf{r}) = \sum_{ik} f^\sigma_{ik} |\Psi^\sigma_{ik}(\mathbf{r})|^2$ (f is the Fermi function and it is evaluated at zero temperature (T=0)). The on-site density matrix is also determined from $|\Psi\rangle$ using for example the method described in Section III B or Section III C. Finally, we require consistency between the ρ^σ and $n^{\tau\sigma}$ and the Kohn-Sham and V_{int} potentials they imply.

Once self-consistent solutions of ρ^σ and $n^{\tau\sigma}$ are obtained, the total ground-state energy E can be obtained from the value of Eq. 1 at the stationary point of both ρ^σ and $n^{\tau\sigma}$. It is also useful to cast the total energy functional in Eq.1 is a slightly different form, both for analysis and for technical reasons specially when using Wannier functions. The SDFT+U total energy functional can be decomposed into the SDFT energy (E^{SDFT}), the KS energy correction ($E^{\Delta KS}$), and the interaction energy correction (E^{int}) (defined only within the correlated subspace) as follows:

$$E = E^{SDFT} + E^{\Delta KS} + E^{int}, \tag{10}$$

where

$$E^{SDFT} = \mathbf{Tr}[\langle \hat{H}^\sigma_{KS} \rangle] - \mathbf{Tr}[\hat{V}^\sigma_{Hxc} \cdot \rho^\sigma] + E^{Hxc}[\rho^\sigma] \tag{11}$$

and

$$E^{\Delta KS} = \mathbf{Tr}[\langle \hat{H}^\sigma_U \rangle] - \mathbf{Tr}[\hat{V}^\sigma_{int} \cdot n^{\tau\sigma}] - \mathbf{Tr}[\langle \hat{H}^\sigma_{KS} \rangle]. \tag{12}$$

DFT+U is a special case of the SDFT+U in which the exchange-correlation energy depends only on the total density ρ, i.e., $\Phi_{KS}(\rho^\sigma) \to \Phi_{KS}(\rho)$. However, spin dependence is retained in the correlated subspace, so $\mathbf{n}^{\tau\sigma}$ is still considered to be spin dependent. Thus the total energy functional in Eq. 1 becomes

$$\begin{aligned} E[\rho, n^{\tau\sigma}] = {} & \mathbf{Tr}[\langle \hat{H}^\sigma_U \rangle] - \mathbf{Tr}[\hat{V}_{Hxc} \cdot \rho] \\ & - \mathbf{Tr}[\hat{V}^\sigma_{int} \cdot n^{\tau\sigma}] + E^{Hxc}[\rho] + E^{int}[n^{\tau\sigma}], \end{aligned} \tag{13}$$

where

$$\hat{H}^\sigma_U = \hat{H}_{KS} + \hat{V}^\sigma_{int}. \tag{14}$$

The rest of the formalism carries through as before, except that the exchange-correlation potential now depends only on ρ and therefore the double counting correction is taken to be spin-independent:

$$E^{DC}[N_\tau] = \frac{U}{2} N_\tau (N_\tau - 1) - \frac{J}{4} N_\tau (N_\tau - 2), \tag{15}$$

implying

$$V_{DC}[N_\tau] = U(N_\tau - \frac{1}{2}) - \frac{J}{2}(N_\tau - 1). \tag{16}$$

Thus in DFT+U theories spin dependence arises only from the properties of the correlated subspace (which affect the rest of the system via hybridization).

III. CORRELATED ORBITALS AND THE IMPLEMENTION OF (S)DFT+U USING THE PROJECTOR-AUGMENTED PLANE WAVE METHOD

A. Overview

In this paper, the DFT portion of the functional (Eq. 11) is implemented using the projector augmented wave (PAW) method[38]. The main idea of PAW is to circumvent treating the computationally inconvenient core states by use of a linear transformation which relates an all-electron wavefunction $|\psi\rangle$ to a pseudo wavefunction $|\tilde{\psi}\rangle$. The transformation requires the addition of augmentation terms which can be expanded using a projector function $|\tilde{p}\rangle$ and the resulting KS Hamiltonian contains additional terms arising from the augmentations, but because the resulting pseudo-wavefunction is smoothly varying computations are much more efficient.

In the PAW method, the SDFT energy functional can be split into three terms:

$$E^{SDFT} = \tilde{E}[\tilde{n}, \hat{n}, \tilde{n}_{Zc}] + E^1[n^1, n_{Zc}] - \tilde{E}^1[\tilde{n}^1, \hat{n}, \tilde{n}_{Zc}] \tag{17}$$

where $\tilde{E}$ is the pseudo-energy term, E^1 is the on-site all-electron energy term, and $\tilde{E}^1$ is the on-site pseudo-energy term. $\tilde{n}$ is the pseudo charge density, n^1 is the on-site all-electron charge density, $\tilde{n}^1$ is the on-site pseudo charge density, $\hat{n}$ is the compensation charge between n^1 and $\tilde{n}^1$ such that $\tilde{n}^1 + \hat{n}$ has the exact same moment as n^1, $\tilde{n}_{Zc}$ is the pseudized core density, and n_{Zc} is the all-electron core density.

The effective $\hat{H}^\sigma_{KS}$ for generating the pseudo wavefunction $|\tilde{\psi}\rangle$ is now given by extremizing E^{SDFT} in Eq. 17 with respect to the pseudized charge $\tilde{\rho}^\sigma$:

$$\hat{H}^\sigma_{KS} = -\frac{1}{2}\hat{\nabla}^2 + \tilde{v}_{eff} + \sum_{i,j} |\tilde{p}_i\rangle(\tilde{D}_{ij} + D^1_{ij} - \tilde{D}^1_{ij})\langle\tilde{p}_j| \tag{18}$$

where $\tilde{v}_{eff}$ is the effective pseudo one-particle potential obtained using $\tilde{v}_{eff} = \frac{\partial E^{SDFT}}{\partial \tilde{\rho}^\sigma}$. $\tilde{D}_{ij}$, D^1_{ij}, and $\tilde{D}^1_{ij}$ are potentials conjugate to the density matrix of the augmentation part ρ_{ij}, ie, $\tilde{D}_{ij} = \frac{\partial \tilde{E}}{\partial \rho_{ij}}$, $D^1_{ij} = \frac{\partial E^1}{\partial \rho_{ij}}$, and $\tilde{D}^1_{ij} = \frac{\partial \tilde{E}^1}{\partial \rho_{ij}}$.

Eq. 17 can be cast into a similar form as Eq. 11:

$$E^{SDFT}[\rho^\sigma] = \sum_{i\mathbf{k}} f_{i\mathbf{k}}\langle\tilde{\psi}_{i\mathbf{k}}|\hat{H}^\sigma_{KS}|\tilde{\psi}_{i\mathbf{k}}\rangle + E^{PAW}_{dc}[\tilde{n}, \hat{n}, n^1, \tilde{n}^1]. \tag{19}$$

The PAW double counting correction E^{PAW}_{dc} also contains a pseudo part and an augmentation part:

$$E^{PAW}_{dc}[\tilde{n}, \hat{n}, n^1, \tilde{n}^1] = \tilde{E}_{dc}[\tilde{n}, \hat{n}] + E^1_{dc}[n^1] - \tilde{E}^1_{dc}[\tilde{n}^1, \hat{n}]. \tag{20}$$

The PAW double counting correction E^{PAW}_{dc} should not be confused with the double-counting correction E^{DC} required in the interaction functional. The derivation of the above equations and the explanation of each term are given in Ref. 39.

The treatment of the +U interactions in the PAW formalism depends on the prescription used to construct the correlated subspace. Accordingly, the remainder of this section is divided into two parts, one dealing with the projector formalism (subsection III B) and one with the Wannier formalism (subsection III C).

B. Projectors: ortho-normalization

We begin with the projector method, in which the components $n^{\tau\sigma}_{mn}$ of the correlated orbital density matrix n appearing in Eq. 1 are obtained by projecting the Kohn-Sham wavefunction ψ onto the spherical harmonics Y_{lm} inside an atomic sphere centered on atom τ with the radius r^τ_c, i.e.,

$$n^{\tau\sigma}_{mn} = \sum_{i\mathbf{k}} f_{i\mathbf{k}}\langle\psi^\sigma_{i\mathbf{k}}|\hat{P}^\tau_{mn}|\psi^\sigma_{i\mathbf{k}}\rangle. \tag{21}$$

Here i is a band index and $\mathbf{k}$ is a wavevector in the first Brillouin zone. $f_{i\mathbf{k}}$ is the Fermi function evaluated at T=0 throughout our paper and $\hat{P}^\tau_{mn}$ is the projector function on atom τ defined by

$$\langle\mathbf{r}'|\hat{P}^\tau_{mn}|\mathbf{r}\rangle = Y^*_{ln}(\hat{\mathbf{r}}'_\tau)Y_{lm}(\hat{\mathbf{r}}_\tau)\delta(r_\tau - r'_\tau)\Theta\left(r_\tau < r^\tau_c\right) \tag{22}$$

where $\mathbf{r}_\tau = \mathbf{r} - R_\tau$ is the position vector defined with respect to the atomic center R_τ and $\Theta(x)$ is the step function such that $\Theta(x) = 1$ if $x < 0$ and $\Theta(x) = 0$ if $x > 0$.[40] Note that if the fermi function is removed from Eq. 21 and the sum is taken over all bands i and momenta $\mathbf{k}$ then standard completeness relations imply that

$$O^{\tau\sigma}_{mn} \equiv \sum_{i\mathbf{k}}\langle\psi^\sigma_{i\mathbf{k}}|\hat{P}^\tau_{mn}|\psi^\sigma_{i\mathbf{k}}\rangle \sim O_n\delta_{mn} \tag{23}$$

is a diagonal matrix, whose normalization depends on the choice r^τ_c of sphere cutoff.

Within the PAW formalism, $n^{\tau\sigma}_{mn}$ is computed from the pseudo-wavefunctions $|\tilde{\psi}\rangle$ and a pseudo-projector $\tilde{P}^{\tau\sigma}$ as

$$n^{\tau\sigma}_{mn} = \sum_{i\mathbf{k}} f_{i\mathbf{k}}\langle\tilde{\psi}^\sigma_{i\mathbf{k}}|\tilde{P}^\tau_{mn}|\tilde{\psi}^\sigma_{i\mathbf{k}}\rangle. \tag{24}$$

The pseudo-projector is defined in terms of an appropriate set $|\phi_a\rangle$ of solutions to the Schroedinger equation for a reference atom in free space as

$$\tilde{P}^\tau_{mn} = \sum_{ab} |\tilde{p}_a\rangle\langle\phi_a|\hat{P}^\tau_{mn}|\phi_b\rangle\langle\tilde{p}_b| \tag{25}$$

where the $|\tilde{p}\rangle$ are the PAW projector functions conjugate to the ϕ_a. In practice, we use the implementation in the VASP code.

The wave functions defined by the PAW projector process do not constitute an orthonormal set because the sum is only over a subset of states and a choice of sphere radius is made. Thus the overlap matrix

$$O^{\tau\sigma}_{mn} = \sum_{i\mathbf{k}}\langle\tilde{\psi}^\sigma_{i\mathbf{k}}|\tilde{P}^\tau_{mn}|\tilde{\psi}^\sigma_{i\mathbf{k}}\rangle \tag{26}$$

is neither diagonal nor possessing correctly normalized eigenvalue. To obtain a properly ortho-normalized density matrix $\bar{n}$ within the correlated subspace we define

$$\overline{n}^{\tau\sigma}_{mn} = \sum_{m'n'} (O^{\tau\sigma})^{-1/2}_{mm'} \cdot n^{\tau\sigma}_{m'n'} \cdot (O^{\tau\sigma})^{-1/2}_{n'n}. \quad (27)$$

This procedure of the ortho-normalization of the projector function is used in some DFT+DMFT implementations[22].

Within the PAW formalism, the effective Hamiltonian $\hat{H}^{\sigma}_{U}$ can be obtained by varying the energy functional Eq. 1 with respect to the pseudized charge $\tilde{\rho}^{\sigma} = \sum_{i\mathbf{k}} f_{i\mathbf{k}} |\tilde{\psi}^{\sigma}_{i\mathbf{k}}\rangle\langle\tilde{\psi}^{\sigma}_{i\mathbf{k}}|$:

$$\hat{H}^{\sigma}_{U} = \hat{H}^{\sigma}_{KS} + \frac{dE^{int}}{d\tilde{\rho}^{\sigma}} = \hat{H}^{\sigma}_{KS} + V^{\sigma}_{int}[\bar{n}^{\tau\sigma}] \cdot \frac{d\bar{n}^{\tau\sigma}}{d\tilde{\rho}^{\sigma}} \quad (28)$$

The $\frac{d\bar{n}^{\tau\sigma}}{d\tilde{\rho}}$ term in Eq. 28 is difficult to evaluate because the overlap matrix O in Eq. 27 also varies implicitly due to the change of $|\tilde{\psi}_{i\mathbf{k}}\rangle$. For simplicity, we assume that the ortho-normalization effect is fully incorporated in the electronic $V^{\sigma}_{int}[\bar{n}^{\tau\sigma}]$ term while the change of the density matrix via $\tilde{\rho}$ is computed from the un-normalized $n^{\tau\sigma}$:

$$\begin{aligned} V^{\sigma}_{int}[\bar{n}^{\tau\sigma}] \cdot \frac{d\bar{n}^{\tau\sigma}}{d\tilde{\rho}} &\simeq V^{\sigma}_{int}[\bar{n}^{\tau\sigma}] \cdot \frac{dn^{\tau\sigma}}{d\tilde{\rho}} \quad (29) \\ &= \sum_{ij} |\tilde{p}_i\rangle \cdot (V^{\sigma}_{int}[\bar{n}^{\tau\sigma}] \cdot \langle\phi_i|\hat{P}^{\tau}|\phi_j\rangle) \cdot \langle\tilde{p}_j|. \end{aligned}$$

This interaction potential part is expanded with the basis of the projector $|p\rangle$ and it can be added to the augmentation part of $\hat{H}^{\sigma}_{KS}$ in Eq. 30. Therefore, the Hamiltonian $\hat{H}^{\sigma}_{U}$ is given by

$$\hat{H}^{\sigma}_{U} = -\frac{1}{2}\hat{\nabla}^2 + \tilde{v}_{eff} + \sum_{i,j} |\tilde{p}_i\rangle(\tilde{D}_{ij} + D^1_{ij} - \tilde{D}^1_{ij} + \overline{V}_{ij})\langle\tilde{p}_j| \quad (30)$$

where

$$\overline{V}_{ij} = V^{\sigma}_{int}[\bar{n}^{\tau\sigma}] \cdot \langle\phi_i|\hat{P}^{\tau}|\phi_j\rangle. \quad (31)$$

The total energy functional within PAW can be obtained as follows:

$$\begin{aligned} E[\rho^{\sigma}, n^{\tau\sigma}] = &\sum_{i\mathbf{k}} f_{i\mathbf{k}} \langle\tilde{\Psi}_{i\mathbf{k}}|\hat{H}^{\sigma}_{U}|\tilde{\Psi}_{i\mathbf{k}}\rangle + E^{PAW}_{dc}[\tilde{n}, \hat{n}, n^1, \tilde{n}^1] \\ &- \mathbf{Tr}(V^{\sigma}_{int}[\bar{n}^{\tau\sigma}] \cdot n^{\tau\sigma}) + E^{int}[\bar{n}^{\tau\sigma}]. \quad (32) \end{aligned}$$

The interaction energy correction E^{int} (E^{pot} (Eq. 3) - E^{DC} (Eq. 4)) term and the interaction potential correction V^{σ}_{int} term are computed using the orthonormalized density matrix $\overline{n}^{\tau\sigma}_{mn}$. In practice, the band energy correction term $\mathrm{Tr}(V^{\sigma}_{int}[\bar{n}^{\tau\sigma}] \cdot n^{\tau\sigma})$ is computed only updating the V^{σ}_{int} term while the density $n^{\tau\sigma}$ is obtained from unnormalized projector functions. In this way properly orthonormalized correlated orbitals can be used with only a slight modification of the PAW formalism.

C. MLWF orbitals

Here, we derive the +U formalism in the case where the correlated subspace $n^{\tau\sigma}_{mn}$ is defined by Wannier functions. We follow the approach used in our previous analysis of the DFT+DMFT formalism[13]. In this subsection we present the formalism purely for DFT+U, as all of the comparisons between projectors and Wannier in this study will take place in the context of DFT+U. The generalization to SDFT+U is however straightforward.

Wannier functions are discussed at length in the literature[33–35]. Here we make only a few remarks. First, the construction of a Wannier functions requires the specification of a hybridization window W, a range of energies from which the states used in the construction of the Wannier functions are defined. This energy range should encompass both the correlated orbitals and the orbitals which directly hybridize with the correlated ones. For example, in the case of the rare-earth nickelates, Wannier functions are constructed from an energy window (≈ 11 eV wide) including the full Ni-3d and O-2p manifolds. By construction the Wannier functions provide a complete orthonormal basis for states within the energy window so it is not necessary to introduce an overlap matrix. A continuous infinity of choices of Wannier basis exists; here we choose a "maximally localized" (MLWF[33]) basis set that minimizes the sum of Wannier function spreads ($\langle r^2\rangle$-$\langle\mathbf{r}\rangle^2$) and also perform an additional orbital rotation as described below Eq. 33 We denote the resulting states as $\left|W^{\mathbf{R}_\tau}_n\right\rangle$ where τ labels an atom within a unit cell, $\mathbf{R}$ denotes a lattice vector, and n is an orbital index.

The projection of the DFT Hamiltonian onto the MLWF basis set is

$$H^{0,\mathbf{R}'_{\tau'}\mathbf{R}_\tau}_{mn} = \langle W^{\mathbf{R}'_{\tau'}}_n|\hat{H}_{KS}|W^{\mathbf{R}_\tau}_m\rangle. \quad (33)$$

As discussed e.g. in Ref. 13, for the Wannier functions pertaining to the correlated states we perform a rotation in the orbital indices to minimize the off-diagonal terms of the on-site correlated-state $\hat{H}^{0,\mathbf{R}_{corr,\tau},\mathbf{R}_{corr,\tau}}_{mn}$ in the mn subspace.

The DFT+U calculation solves the eigenvalue problem of the $\hat{H}_{KS} + \hat{V}^{\sigma}_{int}$ matrix within the hybridization window W. One should note that the $\hat{V}^{\sigma}_{int}$ term is spin-dependent while $\hat{H}_{KS}$ has no explicit spin dependence and has parameters determined by the total density.

The density matrix η within the hybridization window, which includes the correlated subspace as a subset, is obtained from the eigenvalues and eigenfunctions of $\hat{H}_{KS} + \hat{V}^{\sigma}_{int}$ as

$$\eta^{\tau\sigma}_{mn} = \sum_{l\in W,\mathbf{k}} f(\epsilon^{\sigma}_{l\mathbf{k}}) \langle\psi_{l\mathbf{k}}|W^{\mathbf{R}_\tau}_m\rangle\langle W^{\mathbf{R}_\tau}_n|\psi_{l\mathbf{k}}\rangle. \quad (34)$$

The density matrix $n^{\tau\sigma}_{mn}$ in the correlated subspace is a sub-block of $\eta^{\tau\sigma}_{mn}$. Our basis choice in the nm space means that the off-diagonal terms are negligible; $n^{\tau\sigma}_{mn} \approx \delta_{nm}$.

The band energy correction $E^{\Delta KS}$ is then given by

$$E^{\Delta KS} = \mathbf{Tr}(\hat{H}_{KS} \cdot \eta) - \mathbf{Tr}(\hat{H}_{KS} \cdot \eta^0), \qquad (35)$$

where the $\eta^{0,\tau}_{mn}$ is computed via Eq. 34 but using the eigenfunctions and eigenvalues of $\hat{H}_{KS}$ rather than $H_{KS} + V^{\sigma}_{int}$.

The interaction energy can be defined using Eq. 3 with the calculated density matrix (Eq. 34). In our application to the nickelates we construct this term using the Slater-Kanamori Hamiltonian as defined in our previous paper[13] and for ease of reference present the results in the same notation. In Ref. 13 the on-site intra-orbital interaction is given as u, the Hund's coupling is j the inter-orbital interaction is $u - 2j$ and the exchange and pair-hopping terms do not contribute in the Hartree-Fock approximation used here. The parameters are related to the U and J defined elsewhere in the paper by $u = U + (8/7)J$ and $j = (5/7)J$. For the specific application to the nickelates we took u=6.14eV and j=0.71eV (corresponding to U=5eV and J=1eV).

The interaction potential energy is then

$$E^{pot} = u \sum_{m,\tau} n^{\tau\uparrow}_m n^{\tau\downarrow}_m + (u-2j) \sum_{m\neq m',\tau} n^{\tau\uparrow}_m n^{\tau\downarrow}_{m'} + (u-3j) \sum_{m>m',\tau\sigma} n^{\tau\sigma}_m n^{\tau\sigma}_{m'} \qquad (36)$$

while the double counting energy is

$$E^{DC} = \frac{u}{2} N_d(N_d - 1) - \frac{5j}{4} N_d(N_d - 2), \qquad (37)$$

where here N_d is the total occupancy of the d levels on a Ni ion.

IV. THE FORCE FUNCTIONAL

The force functional is defined in terms of the derivatives of the energy functional with respect to atomic positions. Here we present the force functional corresponding to the DFT+U version of the energy functional in Eq. 13; the SDFT+U forces can be derived similarly. The specifics depend on the formalism. As before, the PAW formalism as implemented in VASP is utilized and we present forces for the projector, while we outline the differences for the case of a Wannier based correlated subspace.

The DFT+U force functional consists of two parts, namely the same functional form used in DFT except that the DFT Fermi function is replaced by the DFT+U density matrix utilizing DFT+U eigenvalues and eigenfunctions and an additional force term derived from the E^{int} energy term. The computation of the forces requires consideration of the derivatives of the correlated orbital density matrix with respect to $\mathbf{R}$, which in turn arise from the changes of the correlated orbital wave functions as the atomic positions change. The derivative of the projector orbital is already computed within DFT force formalism, therefore one can adopt the the same calculation already implemented in VASP. In the case of Wannier functions, additional implementation is needed to compute the derivative of Wannier function $|W^{\mathbf{R}}_m\rangle$ with respect to $\mathbf{R}$.

The force functional following from the projector correlated orbital set can be derived from the energy functional in Eq. 32; taking derivatives with respect to $\mathbf{R}$ produces the same functional form as the PAW force functional (see e.g. Ref. 39 for details) except that the eigenvalues ϵ_n and eigenfunctions $\tilde{\psi}_n$ are obtained by solving $\hat{H}^{\sigma}_U$. The force has terms due to the change of the pseudized core charge density $\tilde{n}_{Zc}$ via the explicit movement of the ionic positions, the change of the compensation charge $\hat{n}$ itself, and the change of the projector functions $|\tilde{p}\rangle$ as the ions are moved:

$$F^{DFT+U} = -\sum_n f_n \Big\langle \tilde{\psi}_n \Big| \frac{\partial(\hat{H}^{\sigma}_U - \epsilon_n(1 + \sum_{ij} |\tilde{p}_i\rangle q_{ij} \langle \tilde{p}_j|))}{\partial \mathbf{R}} \Big| \tilde{\psi}_n \Big\rangle = F^1\Big[\frac{\partial \tilde{n}_{Zc}}{\partial \mathbf{R}}\Big] + F^2\Big[\frac{\partial \hat{n}}{\partial \mathbf{R}}\Big] + F^3\Big[\frac{\partial |\tilde{p}\rangle\langle\tilde{p}|}{\partial \mathbf{R}}\Big] \qquad (38)$$

where

$$F^3\Big[\frac{\partial |\tilde{p}\rangle\langle\tilde{p}|}{\partial \mathbf{R}}\Big] = -\sum_{n,ij} (\hat{D}_{ij} + D^1_{ij} - \tilde{D}^1_{ij} + \overline{V}_{ij} - \epsilon_n q_{ij}) \times f_n \langle \tilde{\Psi}_n | \frac{\partial |\tilde{p}_i\rangle\langle\tilde{p}_j|}{\partial \mathbf{R}} | \tilde{\Psi}_n \rangle. \qquad (39)$$

q_{ij} is the correction to the overlap matrix given by $\langle \phi_i | \phi_j \rangle - \langle \tilde{\phi}_i | \tilde{\phi}_j \rangle$. The explicit expressions of F^1 and F^2 are the same as DFT forces given in Ref. 39. The implicit changes of the Hamiltonian H^{σ}_U via the density $\tilde{n}$, n^1, $\tilde{n}^1$, and $\hat{n}$ are always cancelled out exactly against the change of E^{PAW}_{dc} terms in Eq. 32.

The evaluation of a force term from E^{int} requires the derivative of the correlated orbital density matrix, i.e. $\frac{d n^{\tau\sigma}}{d\mathbf{R}}$ and the result depends on the choice of correlated orbital sets. Within the projector scheme, the force term arising from the implicit change of interaction energy correction E^{int} (Eq. 32) via the ortho-normalized density matrix $\bar{n}^{\tau\sigma}$ is given by

$$F^{int} = \frac{dE^{int}[\bar{n}^{\tau\sigma}]}{d\bar{n}^{\tau\sigma}} \cdot \frac{d\bar{n}^{\tau\sigma}}{d\mathbf{R}} = V^{\sigma}_{int}[\bar{n}^{\tau\sigma}] \cdot \frac{d\bar{n}^{\tau\sigma}}{d\mathbf{R}}. \qquad (40)$$

Here, the calculation of $\frac{d\bar{n}^{\tau\sigma}}{d\mathbf{R}}$ term is complicated by the $\mathbf{R}$-dependence of the overlap matrix O (Eq. 27). In practical applications the derivative of the density matrix with respect to the ionic position $\mathbf{R}$ is thus approximated to the change of the un-normalized $n^{\tau\sigma}$ via the derivative of the projector function which is already present in PAW force (Eq. 39):

$$F^{int} \simeq V^{\sigma}_{int}[\bar{n}^{\tau\sigma}] \cdot \frac{dn^{\tau\sigma}}{d\mathbf{R}}. \qquad (41)$$

Taking a derivative of the $-\mathbf{Tr}(V^{int}[\bar{n}^{\tau\sigma}] \cdot n^{\tau\sigma})$ term in Eq. 32 with respect to $\mathbf{R}$ leads to a term $-V^{int}[\bar{n}^{\tau\sigma}] \cdot$

$\frac{dn^{\tau\sigma}}{d\mathbf{R}}$ which cancels out the term in Eq. 41 and a term $-\frac{dV^{int}[\bar{n}^{\tau\sigma}]}{d\mathbf{R}} \cdot n^{\tau\sigma}$ which cancels out the implicit change of $V^{int}[\bar{n}^{\tau\sigma}]$ term in $\hat{H}_U^\sigma$.

The force functional using Wannier functions can be derived in a similar way as the projector functions except that the $\frac{dn^{\tau\sigma}}{d\mathbf{R}}$ term needs to be computed explicitly in terms of the change of Wannier functions with $\mathbf{R}$. However, we have not yet implemented this. Instead, we have determined the minimum energy structure in the phase space of pressure and bond length difference as defined in our previous paper[13].

V. APPLICATION TO STRUCTURAL PROPERTIES OF RARE-EARTH NICKELATES

A. Overview

In following sections we investigate the general issues of interest in this paper, namely different correlated orbital sets (Projector vs Wannier) and background electronic structure methods (DFT+U vs SDFT+U), in the specific context of the structural properties of the rare-earth nickelates, $R\mathrm{NiO}_3$. In these materials the basic structural motif is the NiO_6 octahedron. At some values of temperature, pressure and R, the materials exhibit a uniform phase in which all octahedra have approximately the same mean Ni-O bond length. In other parameter regimes the materials exhibit a two-sublattice disproportionated phase in which the octahedra on one sublattice have a mean Ni-O bond length ~ 0.1Å shorter than the octahedra on the other sublattice. The materials are important for the present study because this basic structural property is closely linked to a fundamental electronic property, namely whether the material is a metal or a correlation-driven site-selective Mott insulator[32,41]. This linkage means that obtaining a correct description of the structural properties poses a critical test for the electronic structure methods.

Our previous studies[12,13] showed that (S)DFT+U does not provide a quantitatively accurate description of the experimental structural and metal-insulator transition phase diagram of $R\mathrm{NiO}_3$ series. A particular difficulty is the prediction that the ambient-pressure ground state of LaNiO_3 is bond-disproportionated and insulating when the actual material has a non-disproportionated $R\bar{3}c$ structure and is metallic. A closely related deficiency of the DFT+U method is an overestimation of the critical pressure of the metal-insulator transition for materials where the ambient pressure ground state is insulating. DFT+DMFT methods produced much better results. It is also the case that DFT+U (and DFT+DMFT) wrongly predict that the ground state is ferromagnetic.

However the trends found in the DFT+U calculations were found to track the trends found in the DFT+DMFT calculations. For example the DFT+U $T \to 0$ structural phase boundary in the pressure-tolerance factor plane was offset by a certain pressume from the DFT+DMFT phase boundary, indicating that the difficulty is simply that the DFT+U methods overestimate (to a considerable degree) the stability of the insulating state. Thus since the aim of the current investigation is understand how different formulations of the theory affect basic issues of structure and energetics, rather than to accurately model material properties, we can use the +U approximation as a flexible and inexpensive computational laboratory with the expectation that the similarity of trends noted above suggests that the general findings will be applicable to DFT+DMFT as well.

We present results computed as described in Appendix A. In the current paper, we use the Vienna Ab-initio Simulation Package (VASP)[39,42] which adopts the PAW formalism. For the exchange-correlation DFT functional, we use a generalized gradient approximation (GGA) with the Perdue-Burke-Ernzerhof (PBE) functional[43] and also adopt a local density approximation (LDA) if necessary. We take the correlated orbitals to be atomic-like Ni-centered d orbitals using the projector method and assume the additional interactions have the form given in Eq. 3. Unless otherwise specified, we use U=5eV and J=1eV for all computations.

We present results for three members of the material family: LuNiO_3 (strong insulator at ambient pressure), NdNiO_3 (insulating but near the phase boundary at ambient pressure), and LaNiO_3 (metallic at ambient pressure). In the rest of this section we introduce the materials and compare the DFT+U and SDFT+U results using both the GGA and LDA functionals for bond lengths and energetics. In the following section we discuss the projector vs Wannier issue and in a third section present implications for computed phase diagrams.

B. Bond disproportionation vs volume

We used the VASP implementation of (S)DFT+U using the GGA functional to perform full structural relaxations of the three compounds from the low-symmetry bond-disproportionated structure with the unit cell volume constrained to take particular values (see Fig. 1). The correlated orbital basis set was treated using the same orthonormalized projector for all calculations (note that the orthonormalization of the basis set required that we modify the VASP energy and force formulas according to Eq. 27). In many cases a disproportionated structure with two inequivalent NiO_6 octahedra was found; for these cases we computed the difference δa in mean Ni-O bond length between Ni sites on different sublattices. Generically if $\delta a \neq 0$ the band structure exhibits a gap at the fermi level (for very small disproportionation amplitudes the gapping may not be complete), but for simplicity of presentation we do not consider the electronic structure here.

Results are shown in Fig. 1. At positive compression ($V - V_0 < 0$) the differences between SDFT+U and

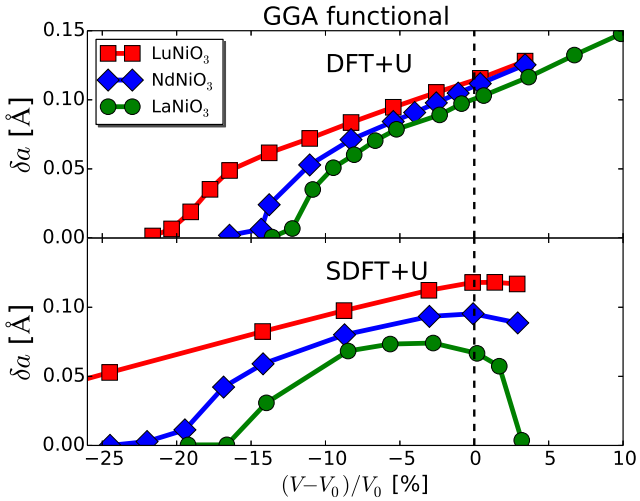

Figure 1. (Color online) Average Ni-O bond-length difference δa as a function of volume computed using the GGA functional with DFT+U (top panel) and SDFT+U (lower panel) for $LuNiO_3$ (red square), $NdNiO_3$ (blue diamond), and $LaNiO_3$ (green circle). U=5eV and J=1eV are used. The same orthonormalized projector method is used to construct the correlated subspace in all cases. V_0 is the zero-pressure volume computed for the given compound by the given method.

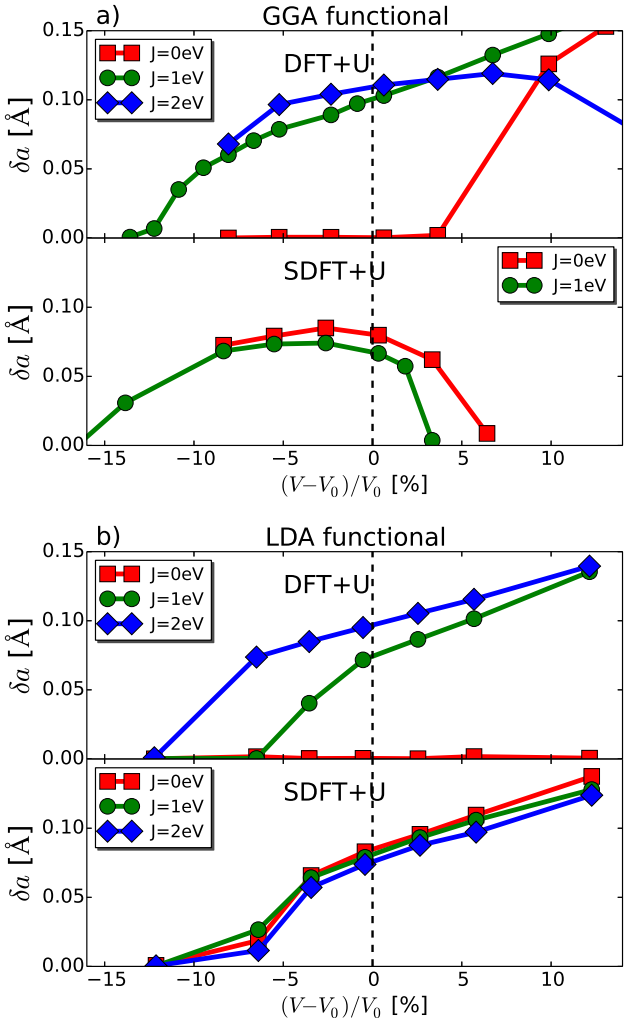

Figure 2. (Color online) Bond disproportionation δa plotted against relative volume change $(V-V_0)/V_0$ computed for $LaNiO_3$ for different Hunds coupling J at U=5eV using both (a) GGA and (b) LDA functionals and different methods indicated in the legends (DFT+U vs SDFT+U). The same orthonormalized projector method is used to construct the correlated subspace in all cases. V_0 is the zero-pressure volume computed using the given method and J=1eV. The change of V_0 at different J is negligible for SDFT+U and rather notable for DFT+U (see Fig. 5) but it does not affect any results discussed here.

DFT+U are quantitative, but large. We see that consistently across the material family SDFT+U predicts a higher δa at given compression and similarly predicts that a higher critical compression is needed to drive the structural transition ($\delta a \to 0$) than does DFT+U. However, at negative compression ($V - V_0 > 0$) the difference is qualitative: DFT+U predicts a monotonic increase of δa values as $(V - V_0)/V_0$ increases while SDFT+U calculations indicate a reduction of δa as the cell volume is increased and ultimately a reentrant structural transition (seen in the data for $LaNiO_3$ and expected for the other materials from the downward curvature).

Fig. 2 shows the effect of varying the Hunds coupling J on the computed bond disproportionation for $LaNiO_3$. In the DFT+U calculations, increasing J from 0 to 1 eV has a dramatic effect, while a further increase to 2 eV has a weaker effect, suggesting a saturation as J is increased. On the other hand, the SDFT+U results show almost no J-dependence, indicating that the spin dependent exchange potential in SDFT already effectively includes a large on-site J and suggesting that J is not needed when performing SDFT+U calculations. This could be problematic for SDFT+DMFT calculations, where the dynamical effect of J are typically important.

The upper portions of the two panels of Fig. 2 further show that within DFT+U the choice of DFT method (LDA vs GGA) produces quantitative but not qualitative differences over the volume range investigated, with in particular the LDA+U exhibiting a smaller δa at given J and volume, consistent with the known tendency of the PBE GGA functional used here to overestimate magnetism[44]. Alternatively, in SDFT+U the choice of DFT method produces a qualitative difference, with the SGGA+U method indicating reentrance of the non-disproportionated phase at a small positive relative volume while no indication of reentrance is found in the LSDA+U calculations.

Interestingly, the J=2eV GGA+U calculations also suggest that reentrance of the undistorted phase would occur at larger relative volumes, consistent with the notion that the SDFT methods imply a large (perhaps ex-

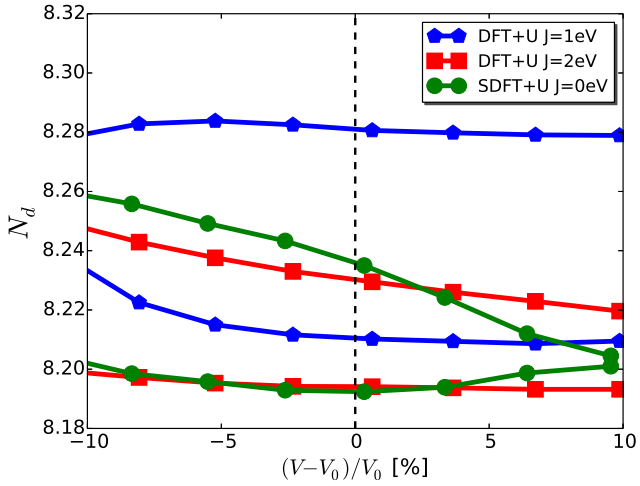

Figure 3. (Color online) The trace of the site-resolved occupancy matrix of the d electrons, N_d per Ni atom computed for $LaNiO_3$ as a function of volume using GGA+U with J=1eV (pentagon dota), J=2eV (square dots) and SGGA+U with J=0eV (circular dots). Two N_d values indicate two Ni atoms with distinct Ni-O bond lengths.

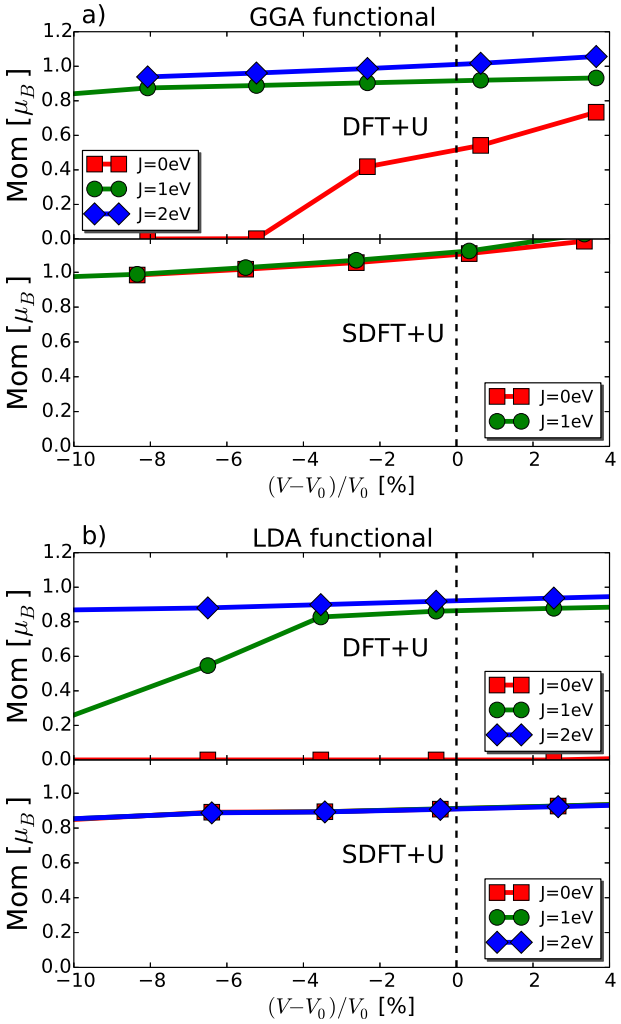

Figure 4. (Color online) The magnetic moments per Ni atom in $LaNiO_3$ obtained using different J as a function of pressure using both (a) GGA and (b) LDA functionals and different methods indicated in the legends (DFT+U vs SDFT+U). The same orthonormalized projector method is used to construct the correlated subspace in all cases. V_0 is the zero-pressure volume computed using the given method and J=1eV.

cessively large) J already at the SDFT level. Taken together these results also suggest that the mathematical origin of the reentrant transition is a (presumably unphysical) effect of large J. The disproportionated phase may be understood as a hybridization density wave corresponding to relatively strong Ni-O bonding at the short-$\delta - a$ site[12] so although the precise connection is not clear at this point we may speculate that the reentrance is related to unphysically large spin-dependence of level shifts of the Ni-d relative to O-p states, weakening the Ni-O singlet bond that produces the distortion.

To elaborate the fact that SGGA+U has a similar effect to GGA+U with a large J, we show in Fig.3 the trace of the site-resolved occupancy matrix, N_d as a function of volume comparing GGA+U with J=2eV (square dots), J=1eV (pentagon dota) and SGGA+U with J=0eV (circular dots). We can see that both SGGA+U with J=0eV and GGA+U with J=2eV produce qualitatively similar physics, i.e., the N_d difference between two Ni ions is reduced as the volume increases and converges to the value of an undistorted structure. The overall behavior is consistent with the qualitative feature of the phase diagram in Fig. 2 (a). Also this is contrary to GGA+U with J=1eV where the N_d difference barely changes for the expanded volume. Nevertheless this reentrant transition occurs rather rapidly for SGGA+U compared to GGA+U with J=2eV. We believe different double counting correction forms in two methods can contribute to this effect, however the detailed analysis of the origin is beyond the scope of our paper.

The interplay between the DFT functional (LDA vs GGA), the value of Hund's J and the physics of the disproportionation instability are also evident in the study of the magnetic moments presented in Fig. 4. The DFT+U results reveal the expected dependence of magnetic moment on J, with magnetic moment increasing with J with the dependence becoming weaker as the saturation value $M = 1\ \mu_B$ is reached and the critical volume for the magnetic transition also being J-dependent. The difference between LDA+U and GGA +U results reflects the stronger tendency toward magnetism characteristic of the PBE-GGA functional. In effect, PBE-GGA already contains a certain degree of local exchange. In contrast, SDFT+U calculations in both GGA and LDA produce large moments at all volumes, and with negligible J dependence.

VI. ENERGETICS

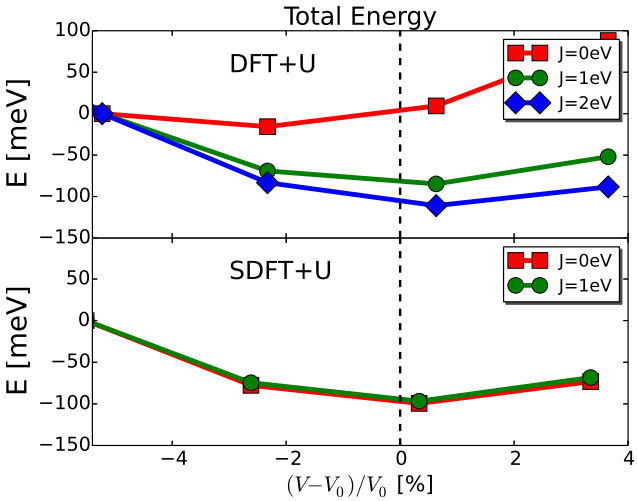

Figure 5. (Color online) The total energy of $LaNiO_3$ as a function of relative volume difference computed using GGA+U (top) and SGGA+U (bottom) with an orthonormalized projector definition of the correlated orbitals at J values indicated. At each volume and for each method the structure is relaxed and the energy of the relaxed structure is presented. The zero of energy is chosen at a compression of 5% in all curves.

In this section, we compare the DFT and SDFT predictions for energies. We restrict attention to the GGA and SGGA density functionals, define the correlated states via orthonormalized projectors, and focus on $LaNiO_3$. For each relative volume, the structure was relaxed and then the energy was evaluated. Fig 5 displays the dependence of the total energy on the normalized volume difference for different J values.

As found in the previous section's analysis of the disproportionation amplitude and magnetic moment, substantial differences between DFT+U and SDFT+U are found. The DFT+U energy curve depends substantially on J, changing rapidly as J is increased from zero and saturating as J becomes large. Remarkably even the equilibrium volume is J-dependent. The SDFT+U energy has negligible J dependence and is similar to the J=2eV DFT+U result again suggesting that the SDFT exchange correlation functional in effect contains a J which (for the PBE-GGA case studied here) is substantially larger than the $J \sim 1$eV values believed to be physically reasonable.

Fig. 6 presents a decomposition of the energy into the DFT contribution (E^{DFT}, panel a) and the correlation correction (CC) contribution ($E^{\Delta KS} + E^{int}$, lower panel), as defined in Eq. 10, for DFT+U (upper half of each panel) and SDFT+U (lower half of each panel). The DFT term E^{DFT} contains the structural contribution while the CC term expresses the correlation physics. E^{DFT} is not monotonic in unit cell volume, expressing

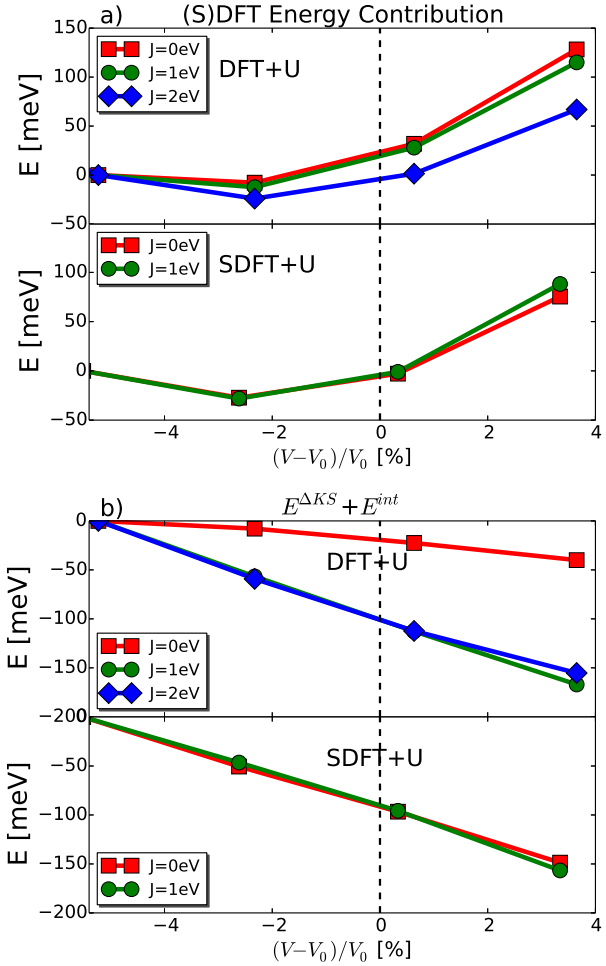

Figure 6. (Color online) Contributions to DFT+U energy functional (cf Eq. 10) computed for $LaNiO_3$ as a function of relative volume. a) The DFT contribution and b) the correlation correction CC contribution ($E^{\Delta KS} + E^{int}$) are decomposed from Fig. 5 using the same relaxed structure at each volume and compared for different methods (DFT+U (the top panel) vs SDFT+U (the bottom panel)) and different J values.

the basic physics of chemical bonding. Alternatively, the CC contribution decreases monotonically as the volume is increased for both DFT+U and SDFT+U and for all J values, expressing the enhancement of correlation occurring when hybridization is decreased and showing that the equilibrium volume predicted by the correlated calculation is larger than that predicted from the DFT contribution alone.

Fig. 6 indicates that for the SDFT+U method neither E^{DFT} nor the CC term has significant J dependence because the SDFT method already includes a large local exchange contribution. Alternatively, in the DFT+U calculation both terms have some J dependence. The DFT+U CC term changes dramatically as J is increased from 0 to 1eV, accounting for the noticeable change of DFT+U energetics from J=0 to 1eV in Fig. 5 but does

not change much as J is further increased because the moment is saturated (see Fig. 4). It is also interesting to note that the DFT+U CC energy at $J \gtrsim 1$eV is comparable to the SDFT+U CC energy at $J = 0$, further confirming the large value of J implicit in the SDFT method. In the DFT+U method, some dependence of E^{DFT} on J occurs as J is increased from 1eV to 2eV, and it is interesting to note that this is the J range where suggestions of reentrance are visible in the DFT+U calculation. This behavior again indicates that the unusual reentrant behavior is related to a rearrangement of the band-structure by an unphysically large Hunds coupling.

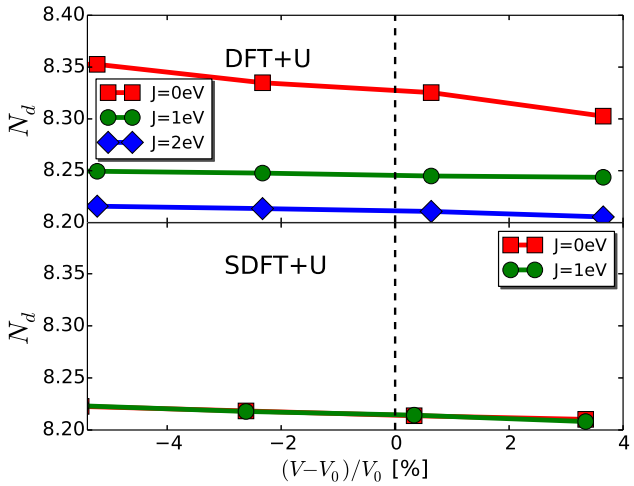

Figure 7. (Color online) The occupancy of the correlated orbitals expressed as the number of d electrons N_d per Ni atom computed for $LaNiO_3$ at J values indicated for GGA+U (the top panel) and SGGA+U (the bottom panel).

As extensively discussed elsewhere[45,46], the occupancy N_d of the correlated orbitals provides useful insights into the physics of strongly interacting electron systems. Fig. 7 displays the d occupancies computed for $LaNiO_3$ for the parameters whose energies are shown in Fig. 6. Within DFT+U, increasing the Hunds coupling J leads to a decrease in N_d, a signal of stronger correlation arising from effectively smaller p-d hybridization. In SDFT+U the correlations in this sense are already stronger at the SDFT level (ie. SDFT+U yields smaller N_d), and adding additional J does not change the situation.

VII. CHOICE OF CORRELATED ORBITAL

In this section we study the effect of the choice of correlated orbital on the calculated results. The DFT+U method is used; SDFT+U is not considered in this section. Fig. 8 presents the bond disproportionation amplitude δa versus reduced volume for different rare earth nickelates using either MLWF (filled symbols, solid lines) or ortho-normalized projectors (open symbols, dashed lines) for the correlated subspace. The qualitative trends of δa as a function of reduced volume are similar for both correlated orbitals. Substantial differences appear only for very large compression, where the Wannier approach enhances the tendency to the bond disproportionated states, though only for $NdNiO_3$ and $LaNiO_3$.

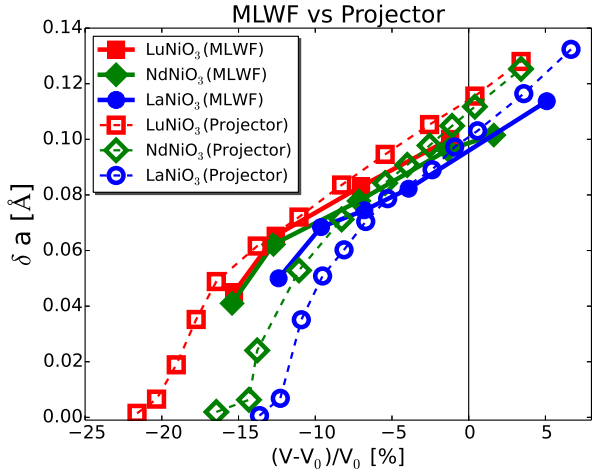

Figure 8. (Color online) The average Ni-O bond length difference δa as a function of reduced volume computed for materials indicated using DFT+U as implemented with the energy functional of Eq. 10. Both maximally localized Wannier functions (filled symbols, solid lines) and ortho-normalized projectors (open symbols, dashed lines)) are compared. Interaction parameters of U=5eV and J=1eV are used for the projector-based calcualtions while the equivalent values u=6.14eV and j=0.71eV (Slater-Kanamori parameterization) are correspondingly used for the Wannier construction.

The origin of the difference is not clear at present, but may have to do with the fact that size of the Wannier function varies as the volume and the bond length difference change, while the projectors are defined using a fixed radius. Fig. 9 displays the Wannier spread for $NdNiO_3$ at $(V - V_0)/V_0 = -12.5\%$ as a function of structural distortion. $NdNiO_3$ at this volume shows noticeably different δa values between for MLWF (∼0.06Å) and for the projector (∼0.03Å). As δa increases, the Wannier orbital for Ni A (large Ni-O octahedron) becomes more localized (smaller spread) and Ni B (small Ni-O octahedron) shows the more delocalized (larger spread) Wannier orbital. Compared to the projectors, therefore, the Ni A site may be more susceptible to the Mott transition and the Ni B electrons are more bound to nearest O holes enhancing a tendency toward the site-selective Mott transition[32]. This difference between the MLWF and the Projector is demonstrated in Fig. 10 for the DFT+U partial density of states computed with the fixed $NdNiO_3$ structure (δa=0.06Å, $(V - V_0)/V_0 = -12.5\%$). The site-selective Mott gap is indeed larger for the MLWF (the top panel) compared to the Projector (the bottom panel), therefore the bond disproportionated structural phase can be energetically more stable for the MLWF. Another difference

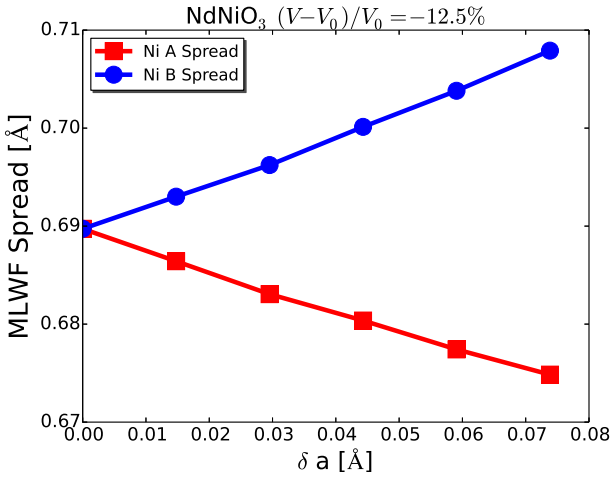

Figure 9. (Color online) The spread of Ni e_g maximally localized Wannier function (MLWF) as a function of the bond length difference δa for $NdNiO_3$ at $(V - V_0)/V_0 = -12.5\%$. Ni A (square dots) means the Ni ion with the longer Ni-O bond length and Ni B (circular dots) means the one with the shorter bond length. The Wannier spread is defined by $\sqrt{(\langle r^2\rangle - \langle r\rangle^2)}$ and the value is averaged over two e_g orbitals.

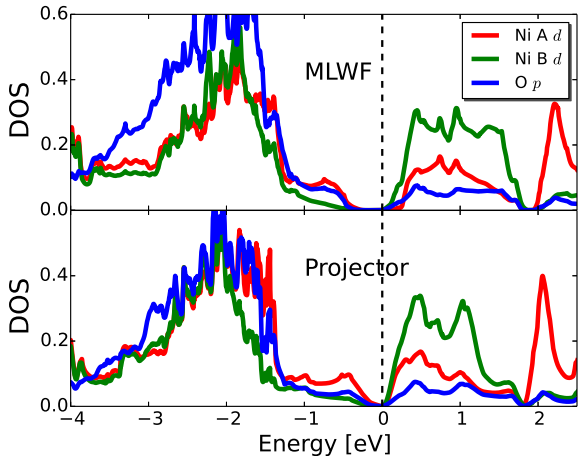

Figure 10. (Color online) The partial density of states for the bond disproportionated $NdNiO_3$ (δa=∼0.06Å, $(V - V_0)/V_0 = -12.5\%$) computed using DFT+U with the correlated orbital of the MLWF (top) and the Projector (bottom). Ni A d (with the longer Ni-O bond length), Ni B d (with the shorter Ni-O bond length), and O p data are shown for comparison. The density of states is spin-averaged for up spin and down spin.

between the MLWF and the Projector is that the leading edges of the site-resolved excitation gaps for the two Ni ions are different in the MLWF while they are almost same for the Projector.

We now turn to the effect of orthonormalization, comparing in Fig. 11 structural relaxation calculations performed using the orthonormalized projector orbital to

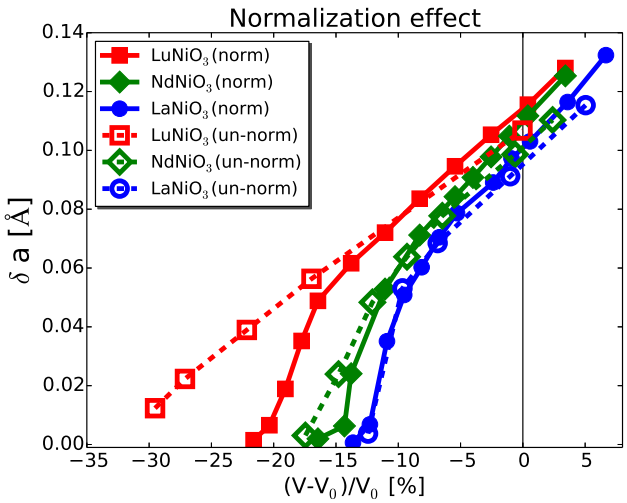

Figure 11. (Color online) Average Ni-O bond length difference δa graph as a function of volumes obtained using DFT+U. The normalization effect of the correlated orbital is investigated by comparing both the ortho-normalized projector correlated orbital (filled symbols, solid lines) and the unnormalized projector (open symbols, dashed lines). $LuNiO_3$ (red square), $NdNiO_3$ (green diamond), and $LaNiO_3$ (blue circle) results are displayed for comparison.

calculations and performed using the unnormalized projector implemented in VASP. Normalization has a particularly important effect in the small volume region of $LuNiO_3$, where the critical pressure calculated using the unnormalized projector is overestimated and probably incorrect. However, normalization has no noticeable effect on the structural relaxation of $LaNiO_3$. As the volume is expanded the consequences of normalization are seen to be minor. This discrepancy in the small volume region may arise from an overestimate of the spectral weight inside the Ni atomic sphere, leading to a mis-estimate of the correlation energy.

VIII. THE PHASE DIAGRAM OF RNIO$_3$ AND THE EQUILIBRIUM VOLUME V_0

In this section, we compute the structural phase digrams and equilibrium volume V_0 of the rare-earth nickelates $RNiO_3$ obtained using DFT+U and SDFT+U as functions of the reduced volume for different R ions. MLWF and project definitions of the correlated orbitals are also explored.

Fig. 12 displays the structural transition phase diagram of rare-earth nickelates $RNiO_3$ in the plane of reduced volume $(V - V_0)/V_0)$ and choice R of rare earth ion computed using the different beyond DFT methods discussed in this paper. The structural transition is between the $P2_1/n$ structure (δa >0) and $Pbnm$ structure (δa=0) for all $RNiO_3$ except rhombohedral $LaNiO_3$. For $LaNiO_3$, the transition associated with the bond-

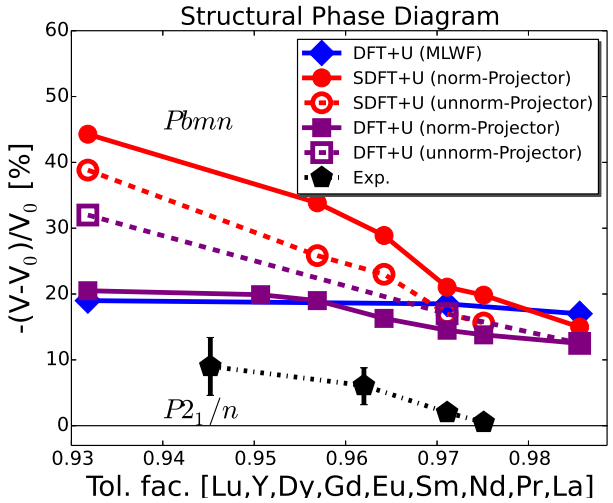

Figure 12. (Color online) Structural phase diagram of the rare-earth nickelates as a function of the volume compression and rare earth ion, computed using DFT+U (square dots) and SDFT+U (circle dots). The un-normalized projector (open dots) and ortho-normalized projector (filled dots) are compared for both methods. The MLWF correlated orbital result (diamond dot) is also shown for DFT+U, yielding some similarity to the phase boundary to the ortho-normalized projector. The experimental data (black dash-dot lines) are also given for comparison[47] (see also Ref. 12 and 13).

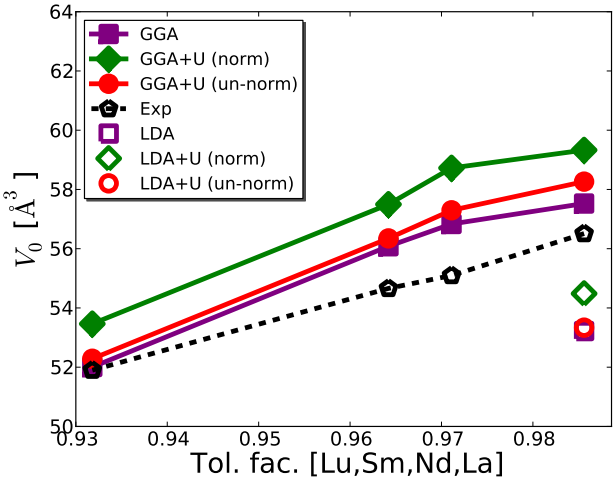

Figure 13. (Color online) Equilibrium volume V_0 calculated using SGGA (filled symbols) and LSDA (open symbols) for RNiO$_3$ with R=La, Sm, Nd and Lu using DFT+U (square dots) and SDFT+U. For SDFT+U, ortho-normalized projector (green diamond) and un-normalized projector (red circle) calculations are compared. The experimental volumes at the ambient pressure are depicted by a black dashed line with open pentagonal dots. LDA(+U) results are shown only for LaNiO$_3$ since the pseudo potentials for other rare earth ions except La are not available.

disproportionation separates the $R3$ structure (δa >0) and the $R\bar{3}c$ structure (δa=0).

All DFT+U and SDFT+U results produce critical compression for the transition which is too large relative to experiment. (DFT+DMFT produces results in much better agreement with experiment[12,13]). The SDFT+U method (red circular dots) exhibits more rapid variation of the critical compression with change of R ions than does DFT+U (purple square dots).

The effect of the ortho-normalization in a correlated orbital varies depending on the functional. SDFT+U implemented using the un-normalized projector as adopted in VASP (circular open dots and dashed lines, also shown in Ref. 12) moderately reduces the critical pressures (favoring the δa >0 region) compared to the same SDFT+U implemented using the ortho-normalized projector (circular filled dots and solid lines). In contrast, DFT+U with the ortho-normalized projector (square filled dots and solid lines) more substantially moves the critical line toward the structural phase with δa=0 ($Pbnm$) for the heavy rare earths.

DFT+U implemented using the MLWF basis set (blue diamond dot and solid line, also shown in Ref. 13 with u=5eV and j=1eV of Slater-Kanamori parametrization) also produces a similar phase boundary to the orthonormalized projector DFT+U calculation compared to other methods. Therefore, we deduce that Wannier and orthonormalized projectors yield similar behavior.

The compression (vertical axis) of the structural phase diagram in Fig. 12 is defined as the relative change of volume compared to the equilibrium volume V_0 computed within each theoretical method. V_0 is determined as the volume of the minimum energy from an energy vs volume curve and the atomic positions at each volume are obtained by minimizing the inter-atomic forces. Results are displayed in Fig. 13 First, we discuss results obtained using pure SDFT within the LSDA and SGGA approximations. The calculated V_0 with GGA exchange-correlation functional (filled symbols) is larger than the experimental one (dashed line), while the V_0 obtained with the LDA exchange-correlation functional (open symbols) is smaller than the experimental value. This behavior is well known in the DFT literature.

We next observe that the calculated V_0 values computed using SDFT+U are rather sensitive to the ortho-normalization of correlated orbitals. The orthonormalized projectors lead to substantially larger equilibrium volumes than the un-normalized projectors, leading to better agreement with experiment for LDA based functionals and worse agreement for GGA, though in neither method is the agreement particularly good.

IX. CONCLUSION

We studied different formulations of DFT+U and SDFT+U in the context of total energy calculations in the rare-earth nickelates. The correlated subspace was

constructed in three different ways: maximally localized Wannier functions, orthonormalized projectors, and non-orthonormalized projectors. We computed the Ni-O bond length difference δa as a function of pressure, the structural phase diagram describing the transition between the bond-disproportionated structure ($\delta a > 0$) and the no bond-disproportionated structure ($\delta a = 0$) as functions of pressure and the rare-earth ions, and also the equilibrium volume.

SDFT+U and DFT+U show qualitatively different behavior in some circumstances. In particular, the SGGA+U results of the structural transition in the rare-earth nickelates show a re-entrant transition with pressure, and this is not observed in GGA+U calculations that are performed with a reasonable on-site exchange $J = 1$eV. However, increasing J to 2eV in GGA+U produced qualitatively similar results to SGGA+U although the re-entrant transition occurs rapidly for SGGA+U, implying that the SGGA spin-polarized exchange correlation functional results in a large effective on-site exchange. SDFT+U based on the LSDA exchange-correlation functional results in a more reasonable effective J, meaning that LSDA+U results using J=0 are similar to LDA+U with $J \sim$1eV. The reentrant transition at negative pressure does not occur within DFT+U calculations using the LDA functional for $J \leq$2eV. Our results suggest that there is no need to use an on-site exchange when performing SDFT+U (ie. set $J = 0$), and this is effectively equivalent to using the approach of Dudarev et al[48]. Additionally, our results imply that the SGGA should be used with caution given its overemphasis of local exchange. More generally, DFT+U with an appropriately chosen J can largely recover the qualitative behavior of SDFT+U.

We demonstrated that orthonormalized projectors behaved rather similarly to MLWF near ambient pressure; although notable differences are evident for $NdNiO_3$ and $LaNiO_3$ under large pressures. Additionally, the un-normalized projector, as implemented in VASP, can lead to notably different results, especially at high pressures. Within SDFT+U, the equilibrium volumes are substantially increased when computed using the orthonormalized orbitals compared to un-normalized orbitals.

Given that (S)DFT+U is equivalent to (S)DFT+DMFT when the DMFT quantum impurity problem is solved within Hartree-Fock, we expect the general findings of this study to be applicable to (S)DFT+DMFT as well. Given our finding that DFT+U with an appropriately chosen J can largely recover the qualitative behavior of SDFT+U, our work supports the long held tradition of basing dynamical mean field extensions on DFT theories rather than SDFT theories. This is particularly important in cases where the dynamical effects of J are crucial. Our results have broad implications for the application of SDFT+U, given that in the nickelates the choice of SDFT functional leads to dramatic differences in the effective on-site exhcange interaction. A very similar conclusion was reached in a study of the spin crossover molecule $Fe(phen)_2(NCS)_2$[49].

Acknowledgements AJM acknowledges support from the Basic Energy Sciences Division of the US Department of Energy under grant ER-046169. HP and CAM acknowledge support from FAME, one of six centers of STARnet, a Semiconductor Research Corporation program sponsored by MARCO and DARPA. This research used resources of the National Energy Research Scientific Computing Center, a DOE Office of Science User Facility supported by the Office of Science of the U.S. Department of Energy under Contract No. DE-AC02-05CH11231.

Appendix A: Computational details

The (S)DFT+U formalism is implemented in VASP using the projector functions $|\tilde{p}\rangle$ as a correlated orbital set. The Hamiltonian for (S)DFT+U is given by Eq. 30, and the total energy and force equations are also derived in Eq. 32 and Eq. 38. However, the VASP implementation adopt the un-normalized density matrix $n^{\tau\sigma}$ as Eq. 24. In the current paper, we compare the VASP implementation to the ortho-normalization of $n^{\tau\sigma}$ to give rise to $\bar{n}^{\tau\sigma}$ as derived in Eq 27. Fortunately, the VASP implementation provides both DFT+U (LDAUTYPE=4) and SDFT+U (LDAUTYPE=1) methods.

For performing the summation of **k** points in the Brillouin zone, we used the tetrahedron method[50]. When using projector correlated orbitals, a **k**-point mesh of $6 \times 6 \times 6$ (for the $Pbnm$ and $P2_1/n$ structures) and $8 \times 8 \times 8$ (for the $LaNiO_3$ $R\bar{3}c$ and $R3$ structures) are used with an energy cutoff of 600eV. When using the Wannier functions as correlated orbitals, **k** points meshes of size $10 \times 10 \times 10$ is used for $Pbnm$ and $P2_1/n$, while $16 \times 16 \times 16$ for $R\bar{3}c$ and $R3$.

* Present Address: Department of Physics, University of Illinois at Chicago, Chicago, IL 60607, USA; hyowon@uic.edu

[1] G. Kotliar, S. Y. Savrasov, K. Haule, V. S. Oudovenko, O. Parcollet, and C. A. Marianetti, Rev. Mod. Phys. **78**, 865 (2006).
[2] P. Hohenberg and W. Kohn, Phys. Rev. **136**, 864 (1964).
[3] W. Kohn and L. J. Sham, Physical Review **140**, 1133 (1965).
[4] R. Fukuda, T. Kotani, Y. Suzuki, and S. Yokojima, Progress Of Theoretical Physics **92**, 833 (1994).
[5] S. K. Ma and B. Brueckne.ka, Physical Review **165**, 18 (1968).
[6] A. V. der Ven, C. A. Marianetti, D. Morgan, and G. Ceder, Solid State Ionics **135**, 21 (2000).

[7] U. Vonbarth and L. Hedin, Journal Of Physics Part C Solid State Physics **5**, 1629 (1972).
[8] R. Rajagopal and J. Callaway, Phys. Rev. B **7**, 1912 (1973).
[9] O. Gunnarsson and B. I. Lundqvist, Phys. Rev. B **13**, 4274 (1976).
[10] M. Rasolt, Phys. Rev. B **16**, 3234 (1977).
[11] M. Rasolt and H. L. Davis, Physics Letters A **86**, 45 (1981).
[12] H. Park, A. J. Millis, and C. A. Marianetti, Phys. Rev. B **89**, 245133 (2014).
[13] H. Park, A. J. Millis, and C. A. Marianetti, Phys. Rev. B **90**, 235103 (2014).
[14] V. I. Anisimov, J. Zaanen, and O. K. Andersen, Phys. Rev. B **44**, 943 (1991).
[15] V. I. Anisimov, F. Aryasetiawan, and A. I. Lichtenstein, Journal Of Physics-condensed Matter **9**, 767 (1997).
[16] O. Bengone, M. Alouani, P. Blöchl, and J. Hugel, Phys. Rev. B **62**, 16392 (2000).
[17] V. I. Anisimov, A. I. Poteryaev, M. A. Korotin, A. O. Anokhin, and G. Kotliar, Journal of Physics: Condensed Matter **9**, 7359 (1997).
[18] A. I. Lichtenstein and M. I. Katsnelson, Phys. Rev. B **57**, 6884 (1998).
[19] S. Y. Savrasov and G. Kotliar, Phys. Rev. B **69**, 245101 (2004).
[20] L. V. Pourovskii, B. Amadon, S. Biermann, and A. Georges, Phys. Rev. B **76**, 235101 (2007).
[21] O. Grns, I. D. Marco, P. Thunstrm, L. Nordstrm, O. Eriksson, T. Bjrkman, and J. Wills, Computational Materials Science **55**, 295 (2012).
[22] K. Haule, C.-H. Yee, and K. Kim, Phys. Rev. B **81**, 195107 (2010).
[23] M. Aichhorn, L. Pourovskii, V. Vildosola, M. Ferrero, O. Parcollet, T. Miyake, A. Georges, and S. Biermann, Phys. Rev. B **80**, 085101 (2009).
[24] O. K. Andersen and T. Saha-Dasgupta, Phys. Rev. B **62**, R16219 (2000).
[25] E. Pavarini, S. Biermann, A. Poteryaev, A. I. Lichtenstein, A. Georges, and O. K. Andersen, Phys. Rev. Lett. **92**, 176403 (2004).
[26] V. I. Anisimov, D. E. Kondakov, A. V. Kozhevnikov, I. A. Nekrasov, Z. V. Pchelkina, J. W. Allen, S.-K. Mo, H.-D. Kim, P. Metcalf, S. Suga, A. Sekiyama, G. Keller, I. Leonov, X. Ren, and D. Vollhardt, Phys. Rev. B **71**, 125119 (2005).
[27] D. Korotin, A. Kozhevnikov, S. Skornyakov, I. Leonov, N. Binggeli, V. Anisimov, and G. Trimarchi, Eur. Phys. J. B. **65**, 91 (2008).
[28] B. Amadon, F. Lechermann, A. Georges, F. Jollet, T. O. Wehling, and A. I. Lichtenstein, Phys. Rev. B **77**, 205112 (2008).
[29] B. Amadon, Journal of Physics: Condensed Matter **24**, 075604 (2012).
[30] Z. Jian-Zhou, Z. Jia-Ning, D. Xiao-Yu, B. Yan, C. Ling-Cang, F. Zhong, and D. Xi, Chinese Physics B **21**, 057106 (2012).
[31] F. Lechermann, A. Georges, A. Poteryaev, S. Biermann, M. Posternak, A. Yamasaki, and O. K. Andersen, Phys. Rev. B **74**, 125120 (2006).
[32] H. Park, A. J. Millis, and C. A. Marianetti, Phys. Rev. Lett. **109**, 156402 (2012).
[33] N. Marzari and D. Vanderbilt, Phys. Rev. B **56**, 12847 (1997).
[34] N. Marzari, A. A. Mostofi, J. R. Yates, I. Souza, and D. Vanderbilt, Rev. Mod. Phys. **84**, 1419 (2012).
[35] A. A. Mostofi, J. R. Yates, Y.-S. Lee, I. Souza, D. Vanderbilt, and N. Marzari, Computer Physics Communications **178**, 685 (2008).
[36] V. I. Anisimov, I. V. Solovyev, M. A. Korotin, M. T. Czyzyk, and G. A. Sawatzky, Phys. Rev. B **48**, 16929 (1993).
[37] M. T. Czyzyk and G. A. Sawatzky, Phys. Rev. B **49**, 14211 (1994).
[38] P. E. Blöchl, Phys. Rev. B **50**, 17953 (1994).
[39] G. Kresse and D. Joubert, Phys. Rev. B **59**, 1758 (1999).
[40] O. Bengone, M. Alouani, P. Blöchl, and J. Hugel, Phys. Rev. B **62**, 16392 (2000).
[41] J. A. Alonso, J. L. Garcia-Munoz, M. T. Fernandez-Diaz, M. A. G. Aranda, M. J. Martinez-Lope, and M. T. Casais, Phys. Rev. Lett. **82**, 3871 (1999).
[42] G. Kresse and J. Furthmuller, Phys. Rev. B **54**, 11169 (1996).
[43] J. P. Perdew, K. Burke, and M. Ernzerhof, Phys. Rev. Lett. **77**, 3865 (1996).
[44] J. P. Perdew, A. Ruzsinszky, G. I. Csonka, O. A. Vydrov, G. E. Scuseria, L. A. Constantin, X. L. Zhou, and K. Burke, Phys. Rev. Lett. **100**, 136406 (2008).
[45] X. Wang, M. J. Han, L. de' Medici, H. Park, C. A. Marianetti, and A. J. Millis, Phys. Rev. B **86**, 195136 (2012).
[46] H. T. Dang, A. J. Millis, and C. Marianetti, arXiv:1309.2995 (2013).
[47] J.-G. Cheng, J.-S. Zhou, J. B. Goodenough, J. A. Alonso, and M. J. Martinez-Lope, Phys. Rev. B **82**, 085107 (2010).
[48] S. L. Dudarev, G. A. Botton, S. Y. Savrasov, C. J. Humphreys, and A. P. Sutton, Phys. Rev. B **57**, 1505 (1998).
[49] J. Chen, A. J. Millis, and C. A. Marianetti, arXiv:1503.03547 [cond-mat.mtrl-sci] (2015).
[50] P. E. Blöchl, O. Jepsen, and O. K. Andersen, Phys. Rev. B **49**, 16223 (1994).